AGU PUBLICATIONS

JGR

Journal of Geophysical Research: Planets

RESEARCH ARTICLE
10.1002/2013JE004488

Special Section:
Results from the first 100 Sols of the Mars Science Laboratory Mission: Bradbury Landing through Yellowknife Bay

Key Points:
- REMS pressure sensor is operating nominally
- New phenomena have been discovered
- Familiar phenomena have been detected

Correspondence to:
R. M. Haberle,
Robert.M.Haberle@nasa.gov

Citation:
Haberle, R. M., et al. (2014), Preliminary interpretation of the REMS pressure data from the first 100 sols of the MSL mission, *J. Geophys. Res. Planets*, *119*, 440–453, doi:10.1002/2013JE004488.

Received 19 JUL 2013
Accepted 21 JAN 2014
Accepted article online 4 FEB 2014
Published online 6 MAR 2014

Preliminary interpretation of the REMS pressure data from the first 100 sols of the MSL mission

R. M. Haberle[1], J. Gómez-Elvira[2], M. de la Torre Juárez[3], A.-M. Harri[4], J. L. Hollingsworth[1], H. Kahanpää[4], M. A. Kahre[1], M. Lemmon[5], F. J. Martín-Torres[2], M. Mischna[3], J. E. Moores[6], C. Newman[7], S. C. R. Rafkin[8], N. Rennó[9], M. I. Richardson[7], J. A. Rodríguez-Manfredi[2], A. R. Vasavada[3], M.-P. Zorzano-Mier[2], and REMS/MSL Science Teams

[1]NASA/Ames Research Center, Moffett Field, California, USA, [2]Centro de Astrobiología (INTA-CSIC), Madrid, Spain, [3]Jet Propulsion Laboratory, California Institute of Technology, Pasadena, California, USA, [4]Finnish Meteorological Institute, Helsinki, Finland, [5]Department of Atmospheric Sciences, Texas A&M University, College Station, Texas, USA, [6]Department of Earth and Space Science and Engineering, York University, Toronto, Ontario, Canada, [7]Ashima Research, Pasadena, California, USA, [8]Southwest Research Institute, Boulder, Colorado, USA, [9]Department of Atmospheric, Oceanic and Space Sciences, University of Michigan, Ann Arbor, Michigan, USA

Abstract We provide a preliminary interpretation of the Rover Environmental Monitoring Station (REMS) pressure data from the first 100 Martian solar days (sols) of the Mars Science Laboratory mission. The pressure sensor is performing well and has revealed the existence of phenomena undetected by previous missions that include possible gravity waves excited by evening downslope flows, relatively dust-free convective vortices analogous in structure to dust devils, and signatures indicative of the circulation induced by Gale Crater and its central mound. Other more familiar phenomena are also present including the thermal tides, generated by daily insolation variations, and the CO_2 cycle, driven by the condensation and sublimation of CO_2 in the polar regions. The amplitude of the thermal tides is several times larger than those seen by other landers primarily because Curiosity is located where eastward and westward tidal modes constructively interfere and also because the crater circulation amplifies the tides to some extent. During the first 100 sols tidal amplitudes generally decline, which we attribute to the waning influence of the Kelvin wave. Toward the end of the 100 sol period, tidal amplitudes abruptly increased in response to a nearby regional dust storm that did not expand to global scales. Tidal phases changed abruptly during the onset of this storm suggesting a change in the interaction between eastward and westward modes. When compared to Viking Lander 2 data, the REMS daily average pressures show no evidence yet for the 1–20 Pa increase expected from the possible loss of CO_2 from the south polar residual cap.

1. Introduction

The Mars Science Laboratory mission (MSL) successfully delivered the Curiosity Rover to the surface of Mars on 6 August 2012 (UTC). The goals of this one Mars yearlong mission are to assess the present and past habitability of Gale Crater, a 150 km wide impact crater located just south of the equator whose central mound of stratified rock is thought to record environmental changes tied to the planet's climate history since the end of the Noachian era ~ 3.5 Gya. To meet these goals, Curiosity carries a payload of 10 instruments, including one designed to assess the present-day environment (see *Grotzinger et al.* [2012] for an overview of the mission and payload). This experiment, called the Rover Environmental Monitoring Station (REMS), consists of a suite of sensors that measure pressure, air and ground temperature, wind, humidity, and UV fluxes. *Gómez-Elvira et al.* [2012] provide a detailed description of the sensors, how they are accommodated on the rover, their prelaunch calibration results, and measurement goals and strategies. The fact that Curiosity resides at the bottom of a large crater in the tropics provides a unique opportunity to sample a different environment than previous landers [*Golombek et al.*, 2012]. J. Gómez-Elvira et al. (Curiosity's Rover Environmental Monitoring Station: The first 100 sols, submitted to *Journal of Geophysical Research*, 2013) describe the REMS instrument performance during the first 100 Martian solar days (sols) of operations.

In this paper we provide a preliminary interpretation of the pressure data acquired during the first 100 sols. A companion paper [*Harri et al.*, 2014] gives details of the pressure sensor, assesses its performance, and provides selected results. In this paper, we expand on their findings with more emphasis on the science the

pressure data reveal. Pressure data are unique in that they contain information on meteorological phenomena ranging in spatial scale from meters to global and on temporal scales from seconds to years. No other meteorological parameter has that capability. After a brief description of the pressure sensor, the REMS observational strategy, and an overview of the data, we focus on specific phenomena starting with small-scale convective vortices and finishing with decadal climate change. Thus, our intent is to survey the results obtained thus far and to provide a preliminary interpretation with enough detail to formulate testable ideas and hypotheses that can be addressed in follow-on studies.

2. REMS Pressure Sensor

Harri et al. [2014] describe the REMS pressure sensors in detail. Here we briefly summarize their main features. Atmospheric pressure is determined by measuring the capacitance between two single-crystal silicon micromachined electrodes (plates). One plate is fixed, while the other is flexible. Thus, changes in pressure change the separation between the plates and hence the capacitance. The advantage of single-crystal silicon is its high stability, which is important for missions of long duration such as MSL.

The REMS pressure sensors are based on the Barcocap (Barocap/Thermocap are registered trademarks of Vaisala Inc.) technology developed by Vaisala Inc., which offers two different types of sensors: a "high-resolution" type (RSP2M) with a short warm-up time (~1 s) and a "high-stability" type (LL) with a longer warm-up time (~150 s). Because capacitance is also a function of temperature, each Barocap has a Thermocap (also developed by Vaisala) to measure its temperature.

The REMS pressure package consists of two oscillators, each having two Barocaps. The two Barocaps in oscillator 1 are high-resolution types. This oscillator is used only for self-calibration and serves as a backup. Oscillator 2, which is used for the science investigations reported here, has one high-stability Barocap plus a high-resolution Barocap. All Barocaps sample at 1 Hz but can be read out at different rates. For oscillator 2 the nominal strategy is to read out the high-stability Barocap every 16 s and the high-resolution Barocap every second. Prelaunch testing has shown that with this strategy the resolution of each of oscillator 2's Barocaps is ~0.2 and the absolute accuracy of the high stability Barocap is <3 Pa. The error sources for the absolute accuracy of a single measurement are due to calibration offset (<1 Pa), drift (<0.5 Pa), hysteresis-induced hour-to-hour repeatability (<1.5 Pa peak to peak), and noise (± 0.15 Pa) (see *Harri et al*., 2014, for details).

We will refer to the readings of Barocaps 1 and 2 in oscillator 2 as PS1 and PS2, respectively. In practice, PS1 is better suited for longer-term phenomena such as the CO_2 cycle, while PS2 is best used for the study of short-term phenomena such as dust devils. Also, the first 3 min of each PS1 session is somewhat contaminated by a warm-up effect. The resulting accuracy error is of the order $<\pm 0.5$ Pa. In this preliminary analysis we have not removed the first 3 min in each session, but the error is so small that it does not affect our conclusions.

3. Observations and Preliminary Interpretation

3.1. REMS Observation Strategy

All REMS instruments acquire data at 1 Hz during a given sampling interval. In "Background" mode, REMS data are acquired for 5 min at the beginning of every hour. In "Extended" mode, additional data are acquired typically in 1 h blocks. The number of extended blocks varies from sol to sol depending on plan complexity, data volume, and power availability. The extended blocks were cycled through local time in order to provide full diurnal coverage every few sols. On some sols only a few extended blocks were possible, but on others as many as eight were uplinked. Thus, the REMS daily downlink varied from approximately 2 to 9 h of 1 Hz data per sol.

3.2. Overview

Measured surface pressures from PS1 for the first 100 sols (sol 0–100 covers solar longitudes from $L_s = 151°$ to $L_s = 208°$) are shown in Figure 1. The main features of this data set are the large diurnal variation and upward trend in the daily average. The large diurnal variation is mainly due to the thermal tide, while the increase in the daily average is due to the addition of CO_2 to the atmosphere from the retreating south polar seasonal cap. MSL landed at a time in the seasonal cycle very close to the expected annual minimum in global mean pressures. Since landing, daily mean pressures increased from 739.8 Pa on sol 10 to 829.8 Pa on sol 100.

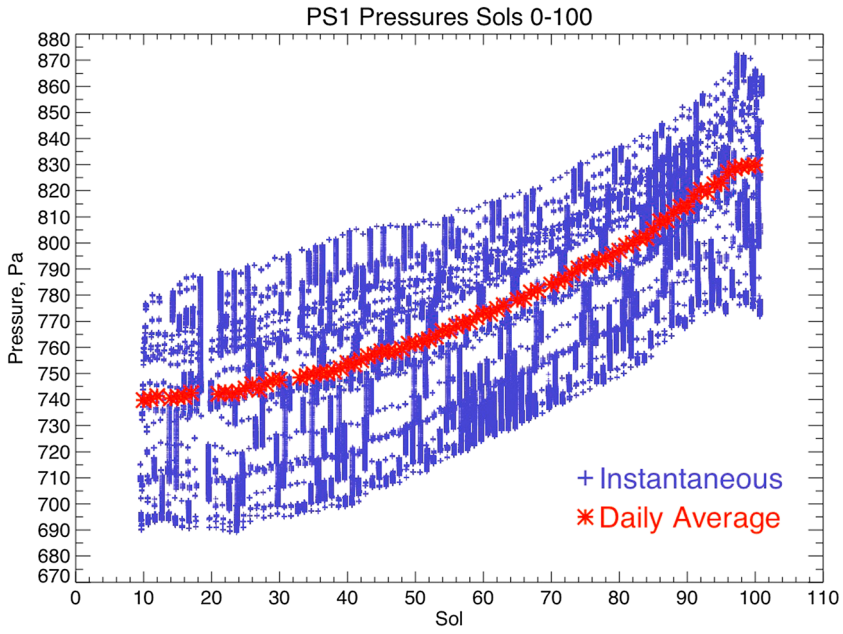

Figure 1. PS1 pressures (blue crosses) and daily averages (red asterisks) for the first 100 sols of the mission. This period covers solar longitudes $L_s = 151°–208°$. Initial checkout activities and software upgrades prevented full daily acquisition of REMS data until sol 9.

The data for each sol presented in Figure 1 (which includes the background and extended sessions) were binned into 1 h intervals. The binned data were then used to compute a daily mean for each sol, which was then subtracted off the value for each hourly bin. The mean diurnal variation of these pressure perturbations for the entire 100 sol period and its first four harmonics are shown in Figure 2. The mean pressure during this period was about 775 Pa with an average diurnal variation of 85 Pa peak to peak. About 85% of that variation is in the diurnal harmonic, which has an amplitude of 36 Pa for this time period. The semidiurnal amplitude is

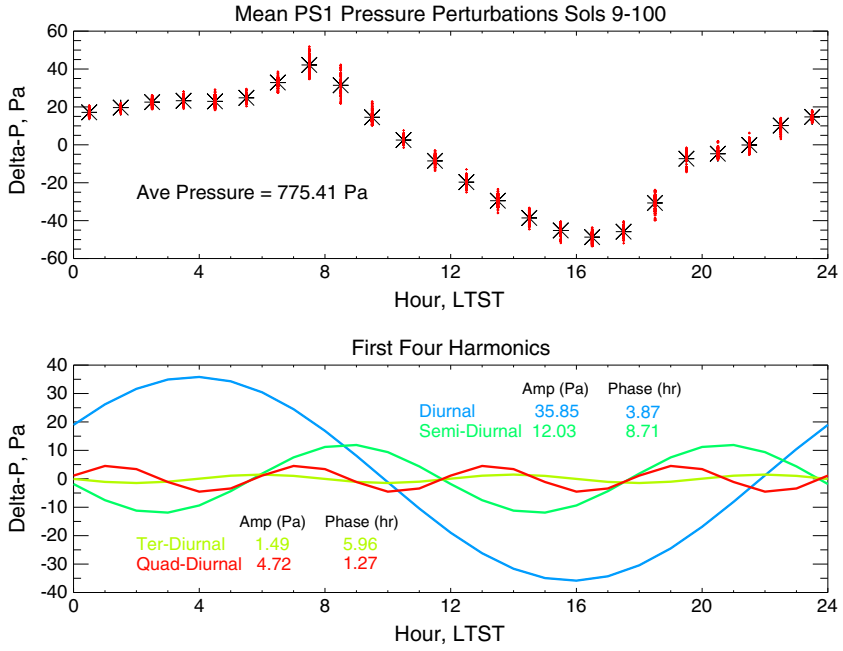

Figure 2. (top) Average pressure departure from the daily mean for the first 100 sols of the mission. Black asterisks are mean values; red dots are actual values and give some idea of the variation during this period. (bottom) Corresponding amplitude and phases of the first four harmonics.

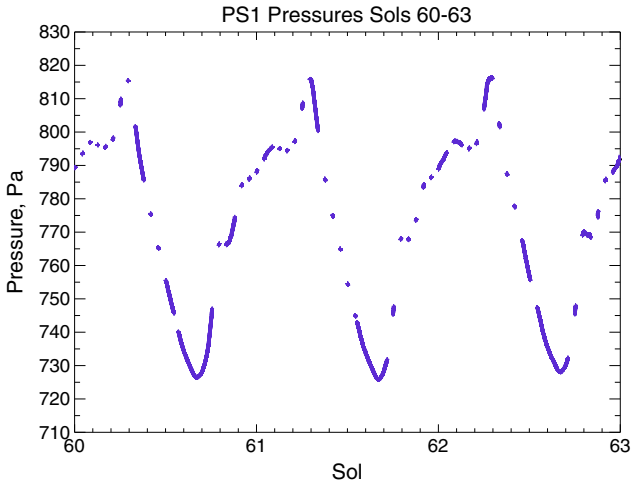

Figure 3. PS1 pressures for sol 60–63.

the next most prominent contributor (12 Pa) followed by the quaddiurnal (4.6 Pa) and terdiurnal (1.3 Pa) tides. The phases, reported here with respect to Local True Solar Time (LTST) (The difference between LTST and Local Mean Solar Time (LMST) was about +35 min on sol 0, increased to about +41 min on sol 66 and then decreased to about +38 min on sol 100), are consistent with that expected from classical tidal theory [e.g., *Wilson and Hamilton*, 1996].

A closer look at selected sols (Figures 3 and 4) reveals some of the details of the diurnal cycle. The extended sessions are clearly visible in these figures and help define the higher-order variations in the diurnal cycle. Maximum pressures occur near 0800 (LTST) and minimum pressures near 1700 (LTST). The maximum is sharply peaked, whereas the minimum is comparatively broad. Secondary local maxima and minima can be seen around 0300 and 2000 with the latter being more sharply defined than the former. These secondary maxima and minima also exhibit more sol-to-sol variability than the primary maxima and minima.

The elevation changes during Curiosity's traverse will lead to pressure changes that need to be assessed. During the first 100 sols of the mission Curiosity drove from Bradbury Landing to Rocknest with several stops along the way. Curiosity reached Rocknest on sol 52 and remained there through sol 100. The straight-line distance between Bradbury Landing and Rocknest is ~330 m, and the total elevation change is ~16 m. Elevation changes associated with this traverse are shown in Figure 5, and estimates of the associated hydrostatic pressure changes are shown in Figure 6. These estimates use a mean pressure of 775 Pa and assume scale heights corresponding to the typical minimum (195 K), maximum (275 K), and average (225 K) air temperatures measured by REMS during this period. Given the absolute accuracy of the sensors (<3 Pa), these changes can be neglected in the analysis that follows.

We present the next set of observations in order of increasing scale beginning with the smallest temporal and spatial scales detectable (seconds/meters) and finishing with the largest scales possible (years/global).

3.3. Convective Vortices

The smallest scales of interest are the sharp pressure drops of up to several pascals over the course of tens of seconds [*Rennó et al.*, 1998, 2000]. Since these drops are observed during midday when surface heating is near its maximum value, we refer to them as convective vortices. Furthermore, these vortices may or may not contain dust. If they do contain dust, they are commonly referred to as dust devils. Thus, convective vortices and dust devils have the same pressure signature and are distinguished only by their dust content. It is worth noting that such vortices appear in large-eddy simulations of the Martian boundary layer [e.g., *Toigo et al.*, 2003; *Michaels and Rafkin*, 2004; *Spiga and Forget*, 2009]. An example of one such vortex using PS2 data is given in Figure 7. These data were acquired on sol 60 shortly before 1:00 P.M. LTST. In some instances, as in Figure 7, these pressure drops are anticorrelated with temperature fluctuations. Unfortunately, REMS wind data are not yet fully reduced though in many cases there does appear to be an abrupt change in the wind direction that is coincident with the pressure drop.

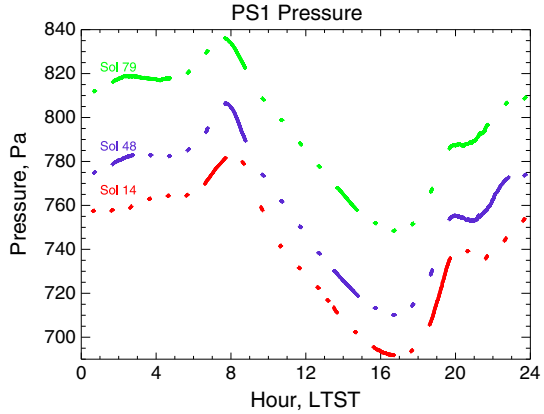

Figure 4. PS1 pressures for sols 14, 48, and 79.

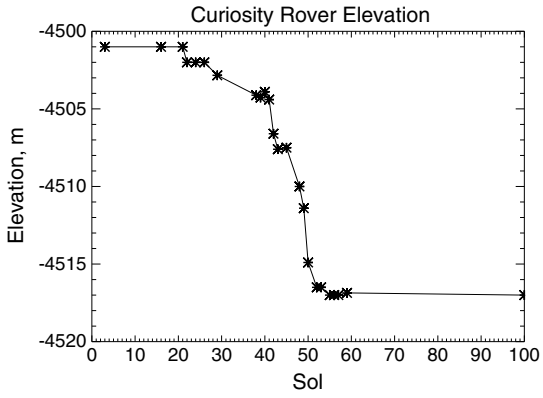

Figure 5. Elevation of Curiosity for the first 100 sols.

The signature of these pressure drops is similar to that seen by Mars Pathfinder [*Schofield et al.*, 1997; *Rennó et al.*, 2000] and the Phoenix Lander [*Ellehøj et al.*, 2010], which were generally interpreted to be the result of dust devils, i.e., convective vortices with entrained dust. Analysis of frequency, intensity, and time of occurrence of the REMS vortices indicates they are similar to the dust devils observed by Pathfinder and Phoenix [*Kahanpää et al.*, 2013]. Based on the REMS analysis, a density of ~200 dust devils per km^2 between 11:00 and 12:00 LMST (~11:40–12:40 LTST at this season) is expected [*Kahanpää et al.*, 2013]. However, high-frequency imaging by Curiosity over a broad area has detected only one plausible dust devil candidate during the first 100 sols [*Moores et al.*, 2013], and dust devil tracks in Gale are virtually absent in orbital images (F. Calef, personal communication, 2013). This, and the fact that for only one of the pressure drops was there a coincident drop in the UV flux, suggests that the convective vortices detected in the REMS pressure data are relatively dust free. Given that dust is abundant on the crater floor, this implies that the vortex winds are not strong enough to raise dust or that the dust in Gale is difficult to mobilize.

An important modeling result related to this observation is the suppression of the daytime boundary layer depth [see *Tyler and Barnes*, 2013]. This suppression is the direct result of the crater circulation, which is upslope along the crater rim and Mount Sharp during the day with general sinking motion in between. This sinking motion keeps the daytime boundary layer confined to below 2 km over the crater floor as compared to 5–10 km outside the crater. Given that the efficiency of converting the surface heat flux into the work of driving dust devils is related to the depth of the boundary layer [*Rennó et al.*, 2000], the crater circulation might be reducing the ability of convective vortices to raise dust.

3.4. Evening Oscillation

The high precision of the REMS pressure sensors, the high sampling frequency of the measurements (1 Hz), and the ability to acquire data for extended periods of more than an hour have led to the detection of a new phenomenon in the pressure data, which we term the "Evening Oscillation." This oscillation is seen in the early evening hours between approximately 1930 and 2230 LTST for those sols for which extended sessions were possible. Figure 8 shows the PS2 data for the first 100 sols during this time period where on almost every sol with an extended session this oscillation is subtle but noticeable. A specific example from sol 48 is given in Figure 9. For this example, we fit the data with a quadratic and subtracted the fit from the data to reveal the amplitude and period of the oscillation, which are ~0.5 Pa and 5–10 min, respectively.

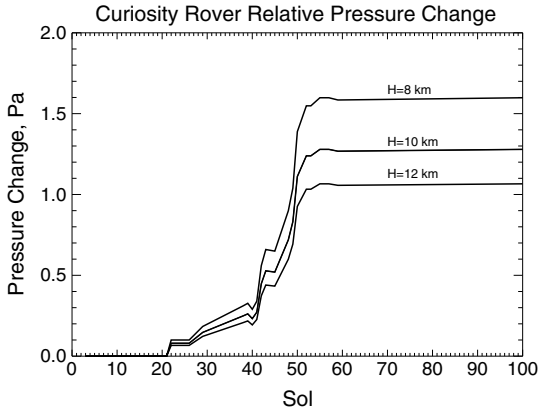

Figure 6. Hydrostatic pressure changes associated with the elevation changes in Figure 5 for a representative range of scale heights *H*.

A plausible interpretation of this oscillation is that it is due to internal gravity waves excited by downslope flow. Internal gravity waves, in this case best approximated by shallow water theory, can exist in stably stratified flows that have a free surface or an internal density discontinuity [e.g., *Holton*, 2004]. At night, the strong cooling along the slopes of the crater rim and Mount Sharp can lead to the development of a shallow layer (~100 m) of high-density fluid underlying a deeper layer of lower density fluid. At the boundary of these fluids a discontinuity develops upon which gravity waves can propagate. The phase speed for such waves is $c = u \pm \sqrt{(gH\,\delta\rho/\rho)}$, where u is the mean downslope wind, g is gravity, H the fluid depth, and $\delta\rho/\rho$ is the normalized density difference

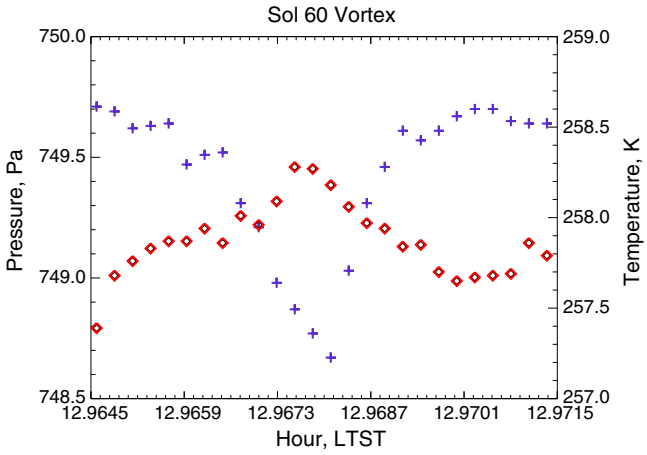

Figure 7. PS2 pressure data (blue crosses) and Boom 1 air temperatures (red diamonds) for a 26-second period shortly before 1300 on sol 60.

between the two layers, which can be approximated by $\delta\rho/\rho \sim 1 - T_1/T_2$, where T_1 and T_2 are the temperatures of the lower and upper layers, respectively. Taking $u = 10\ \mathrm{m\ s^{-1}}$, $H = 100$ m, and $T_1 = 190$ K, $T_2 = 200$ K, we estimate the gravity wave phase speed to be in the range of 5–15 $\mathrm{m\ s^{-1}}$. Given that the observed period of the oscillation is 5–10 min, this suggests a horizontal wavelength between 1.5 and 9.0 km, which is commensurate to the depth of the crater. Since low-amplitude gravity waves are linear and hydrostatic, the perturbation pressure amplitude (0.5 Pa) suggests a height variation of the shallow near-surface layer of $p'/\rho g = 0.5\ \mathrm{Pa}/(2 \times 10^{-2}\ \mathrm{kg\ m^{-3}} \times 3.7\ \mathrm{m\ s^{-2}}) \sim 7$ m, which is much less than the assumed depth of the stable layer. Thus, the amplitude, wavelength, and depth of the near-surface layer are consistent with shallow water theory. A possible explanation for why these oscillations damp out after 2200 is that shear-induced turbulence develops in the near surface layer as the winds become stronger. We emphasize, however, that this is one plausible explanation of the evening oscillation and recognize that other mechanisms, such as flow instabilities, may be at work.

3.5. Crater Circulation Signatures

There are several possible signatures of the crater circulation in the pressure data. The first is the large diurnal variation. Some fraction of that variation must be due to the crater circulation since the upslope/downslope flows induced by the crater should have an impact on measured surface pressures. While the presence of these flows has yet to be confirmed (Curiosity is not close enough to Mount Sharp or the crater rim to detect them with certainty), a variety of atmospheric models predict that they exist and are quite strong [*Vasavada et al.*, 2012; *Tyler and Barnes*, 2013; *Haberle et al.*, 2013; *Harri et al.*, 2014]. During the day the upslope flow along the slopes of Mount Sharp and the walls of the crater rim exports air from the crater floor lowering overall surface pressures. At night downslope flow returns this air thereby raising surface pressures. The phase of this process is roughly coincident with the diurnal tide, and therefore, it should amplify the daily variation of surface pressure.

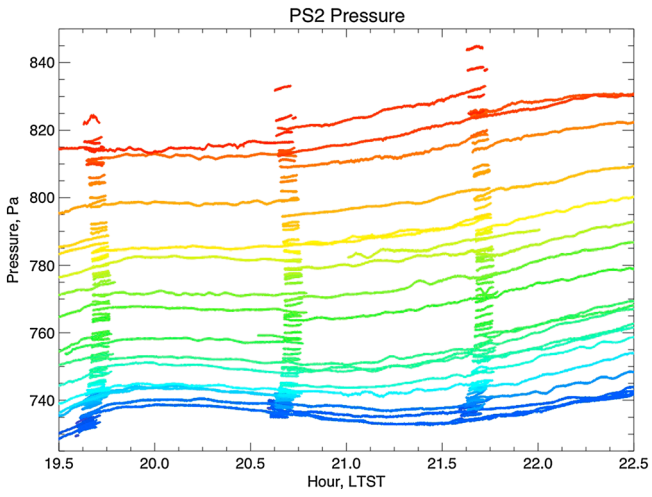

Figure 8. PS2 pressures for sols 9–100 during the period from 19:30 to 22:30. Colors progress from blue on sol 9 to red on sol 100.

The amount of amplification is difficult to assess since it is difficult to isolate circulation effects from hydrostatic (altitude) effects. To illustrate the difficulty, consider the mesoscale modeling simulations of *Tyler and Barnes* [2013] which show a near doubling of the normalized diurnal pressure variation at the bottom of Gale Crater compared to a nearby location in relatively flat terrain just outside the Crater but at a higher elevation [see *Tyler and Barnes*, 2013, Figure 8]. Part of the increased variation is due to the increase in surface pressure with depth into the crater. To the extent the atmosphere is hydrostatic, the increase will be exponential depending

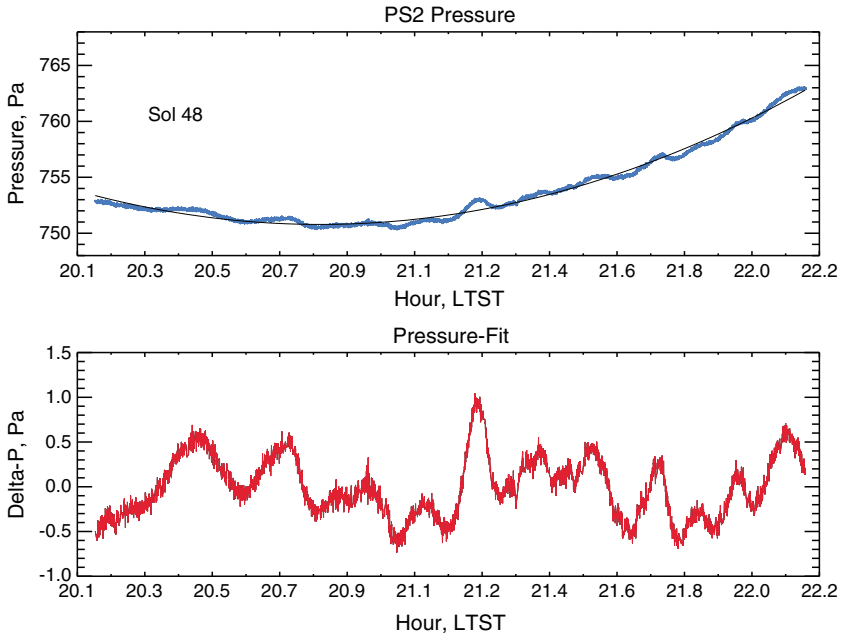

Figure 9. (top) PS2 pressure for sol 48 between 20.1 and 22.2 h (blue curve) and a quadratic fit to this data (thin black line). (bottom) Data fit.

on the thermal structure of the atmosphere. Since diurnal temperature variations increase as the surface is approached, and since the relationship between pressure and temperature is nonlinear, the amplitude of the pressure variations will also increase just due to this hydrostatic effect.

There are several ways to separate the hydrostatic effect from the circulation effect. One is to use surface pressures from a general circulation model (GCM) that does not resolve the crater circulation, hydrostatically adjust them to the elevation of interest, and then compare the adjusted pressures to the observed pressures. In Figure 10 we show results from the Ames GCM which runs at 5° by 6° (latitude/longitude) horizontal resolution and is therefore too coarse to resolve the crater circulation. At the grid point closest to Gale, GCM surface pressures give a peak-to-peak variation of ~40 Pa compared to ~95 Pa measured by REMS at the beginning of the mission. However, the elevation of this grid point is ~3.4 km higher than Curiosity. When model surface pressures are hydrostatically adjusted to Curiosity's elevation, the predicted variation is increased but still less than observed. The difference, ~ 15 Pa, could be attributed to the crater circulation.

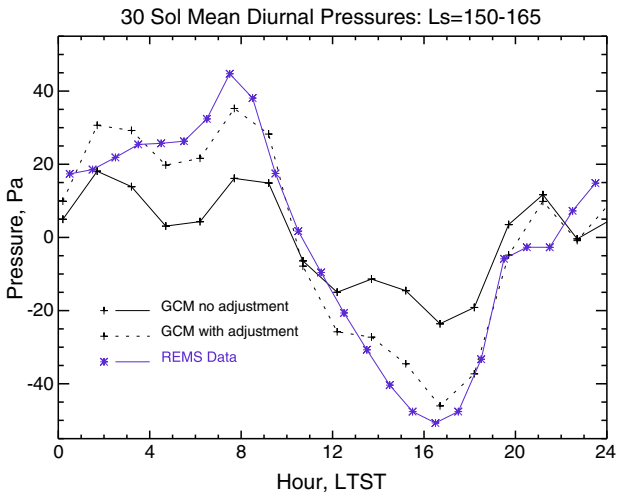

Figure 10. Thirty sol mean diurnal pressures from the Ames GCM (black lines with crosses) and REMS PS1 (blue line with asterisks). The data were binned into 24 one Mars hour periods. GCM results are sampled every hour and a half. Solid black line is for actual surface pressures at the GCM grid point elevation (−1107 m). Dotted black line is for surface pressures hydrostatically adjusted to Curiosity's elevation (−4501 m).

Of course, a major problem with this approach is not knowing a priori what temperature profile to use for the 3.4 km between the grid point elevation and Curiosity's elevation. The adjustment shown in Figure 10 is performed at each model time step and uses scale heights calculated from temperatures at ~ 1 km above the surface. Several other methods were tested but gave poorer results. For the first 30 sols of the mission this approach

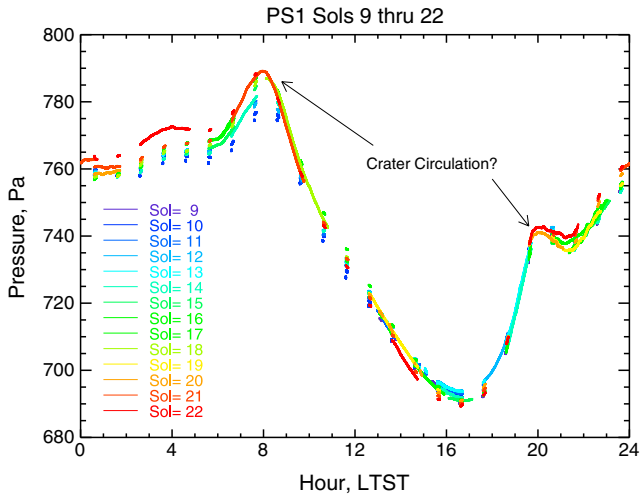

Figure 11. Diurnal pressure variations for the first 14 sols of REMS observations.

gives a diurnal variation of 80 Pa (compared to 95 Pa from REMS) and a daily mean of 742 Pa (compared to 745 Pa from REMS). These are reasonable results, but there is no way of knowing whether they accurately represent the true hydrostatic effect.

Another way to separate the effects is to use a mesoscale model that does simulate the crater circulation and then estimate its contribution by removing the hydrostatic effect. This is opposite the approach just described. *Tyler and Barnes* [2103] take this approach using the Oregon State University Mars Mesoscale Model running at ~5 km horizontal resolution and remove the hydrostatic effect by plotting pressures at each grid point as a function of grid point altitude. They then fit the results to an exponential and subtract the fit from the data to get an estimate of the circulation effect. By averaging over the domain, over many sols (20) and over time of day, they also remove the diurnal cycle that contains the unmodified tidal component. They find that at the floor of the crater where Curiosity landed, the circulation enhances the peak-to-peak diurnal variation by ~20 Pa, a result consistent with the above GCM estimate. These two approaches suggest that between 15 and 20 Pa of the observed daily variation is due to the crater circulation, which is also consistent with the magnitude of pressure perturbations observed in craters by the Mars Express Observatoire pour la Minéralogie, l'Eau, les Glaces et l'Activité (OMEGA) instrument [*Spiga et al*., 2007].

Other possible signatures of the crater circulation are the sharply peaked higher-order features near 0800 LTST and 2000 LTST. These features are shown in Figure 11. They consist of a sharply peaked maximum at 0800 LTST and a localized maximum/minimum between 2000 and 2100 LTST. Such features are not seen in global models, which suggests that they could be the result of the crater circulation. On the other hand, some higher-order features are present in the Ames GCM (see Figure 10), though they are broad and the quaddiurnal component is clearly much too strong (note the obvious presence of four maxima). These features are obviously the result of a global rather than a regional component. Mixed results can also be seen in the mesoscale simulations reported in *Haberle et al*. [2013]. Thus, it is not clear to what extent the observed sharply defined higher-order features present in Figure 11 are due to the crater versus the global circulation. More detailed modeling will be required to sort this out.

3.6. Thermal Tides

The amplitudes and phases of the first four tidal harmonics are shown in Figure 12. Overall, these amplitudes are much larger than those recorded at the Viking, Pathfinder, and Phoenix lander sites. This is due to Curiosity being in a near-equatorial location where tidal forcing (atmospheric heating) is strong, to differences in zonal mean topography, and to the fact that Curiosity is located in a longitude sector where constructive interference of eastward and westward modes is expected [*Wilson and Hamilton*, 1996; *Haberle et al*., 2013]. For the diurnal tide, an additional local enhancement from the crater circulation is also likely [*Tyler and Barnes*, 2013]. The phases of the tides are consistent with classical theory, which predicts a maximum somewhat earlier than 0600 LTST in the tropics for the Sun-synchronous diurnal tide. However, nonmigrating tidal components can produce notable changes in tidal phases. REMS data are showing a phase for the diurnal tide of around 0400 LTST, about 2 h earlier than that expected for the migrating tide. Since diurnal tidal modes have short vertical wavelengths and propagate vertically in the tropics, they are sensitive to the depth and magnitude of localized dust heating. For the semidiurnal tide, whose dominant mode also propagates but has very long vertical wavelengths, classical theory predicts the first maximum around 0900 LTST, which is very close to REMS observations. This tidal component is more sensitive to the total global heating [*Zurek*, 1976; *Leovy and Zurek*, 1979; *Wilson and Hamilton*, 1996].

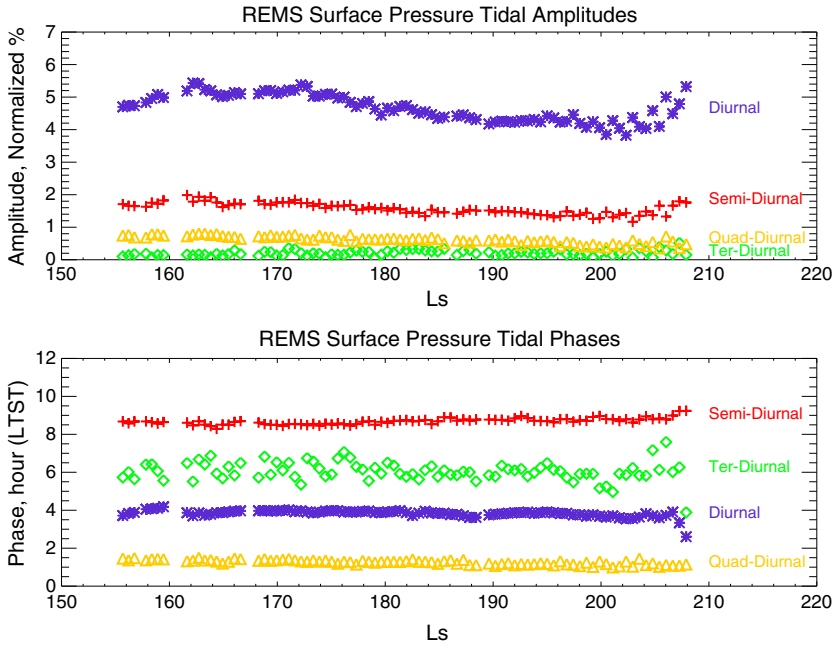

Figure 12. (top) Amplitudes and (bottom) phases of the first four tidal harmonics for the first 100 sols of the mission. Blue asterisks = diurnal; red crosses = semidiurnal; green diamonds = terdiurnal; and gold triangles = quaddiurnal.

Several additional features of the observed tides are worth noting. These are the declining amplitudes from about $L_s = 170°$ to $L_s = 200°$ and then their steady increase after $L_s = 200°$. The latter is also accompanied by a noticeable change in phase. The declining amplitudes could be the result of a declining dust loading. Figure 13 shows the amplitude of the semidiurnal component along with the observed dust loadings at Gale, Mars Exploration Rover-B (MER-B), and Thermal Emission Imaging System (THEMIS). The Gale observations do show a slight downward trend in the opacity, while those at MER-B are rather steady throughout the period. However, the THEMIS opacities, which are global averages, generally trend upward after $L_s = 170°$. Given the sensitivity of the semidiurnal tide to global dust loading, its declining amplitudes are opposite the expectation based on the observed dust opacities alone.

An alternative explanation for the declining amplitudes between $L_s = 170°$ and $L_s = 200°$ is that the Kelvin wave contributions are waning at this season. For uniformly mixed dust, the dominant diurnal and semidiurnal Kelvin modes are particularly strong during early northern summer but decline to about one third of their peak values by fall equinox [see *Wilson and Hamilton*, 1996, Tables 1 and 2]. Whether this is indeed the explanation will require some detailed modeling studies to assess the sensitivity of the Kelvin wave response to nonuniform dust loadings and/or water ice clouds. The latter are prominent in the tropics during northern summer, and their radiative effects are known to be significant at this season [*Wilson et al.*, 2008; *Madeleine et al.*, 2012]. Such studies will place useful constraints on the distribution and optical depth of clouds and dust.

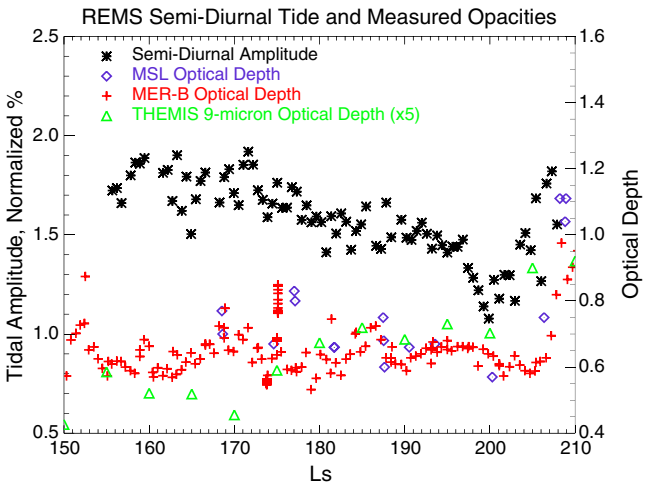

Figure 13. Semidiurnal tidal amplitudes and dust opacities from several sources for the first 100 sols of mission operations.

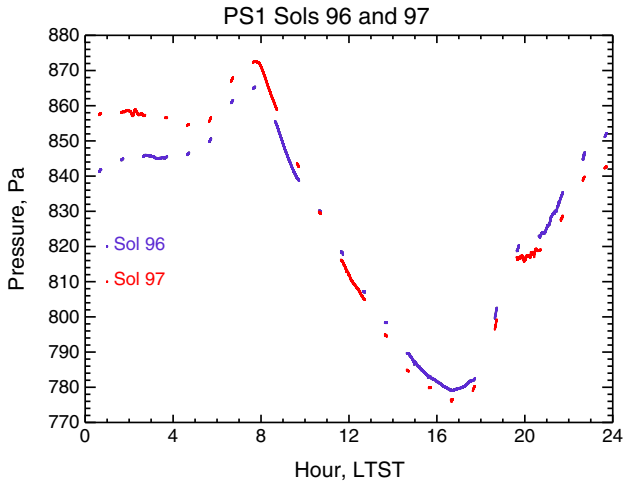

Figure 14. PS1 pressure for sols 96 (blue) and 97 (red) illustrating the onset of the regional dust event described in the text.

The behavior of the tides after $L_s = 200°$ is due to a regional dust lifting event. This event was first detected in the pressure data on sol 97 ($L_s = 207°$) when early morning pressures were significantly elevated with respect to the previous sol (Figure 14). Subsequent observations a few sols later by the Mars Color Imager and the Mars Climate Sounder on the Mars Reconnaissance Orbiter confirmed that widespread dust lifting in the southern hemisphere was occurring and that it was affecting atmospheric temperatures (B. Cantor and D. Kass, personal communication, 2013).

An extension of the time series out to $L_s = 220°$ (sol 120) for the tides is shown in Figures 15 and 16 along with those observed by Viking Lander 1 (VL-1) during its first year of observations in 1977. In both data sets amplitudes increase after $L_s = 200°$ and peak around $L_s = 210°$. However, the storm affecting the VL-1 tides was much larger and more global in extent and raised tidal amplitudes there by a much greater amount. *Zurek* [1981] estimated global visible opacities for this storm of ~2–3 compared to ~0.5 from THEMIS data (assuming a visible/infrared scaling of 2.5 in Figure 13). Rapid changes in phase are also evident in both data sets, except for the semidiurnal tide at VL-1 which was relatively unaffected by the storm. At Gale both tidal components experience phase changes of up to several hours though in opposite directions, and the diurnal phase at Gale changes opposite to the change at VL-1. We attribute these phase changes to changing interactions between the eastward and westward tidal components driven by the changing longitudinal distribution of dust and atmospheric heating. Again, future modeling studies will elucidate the nature of these interactions.

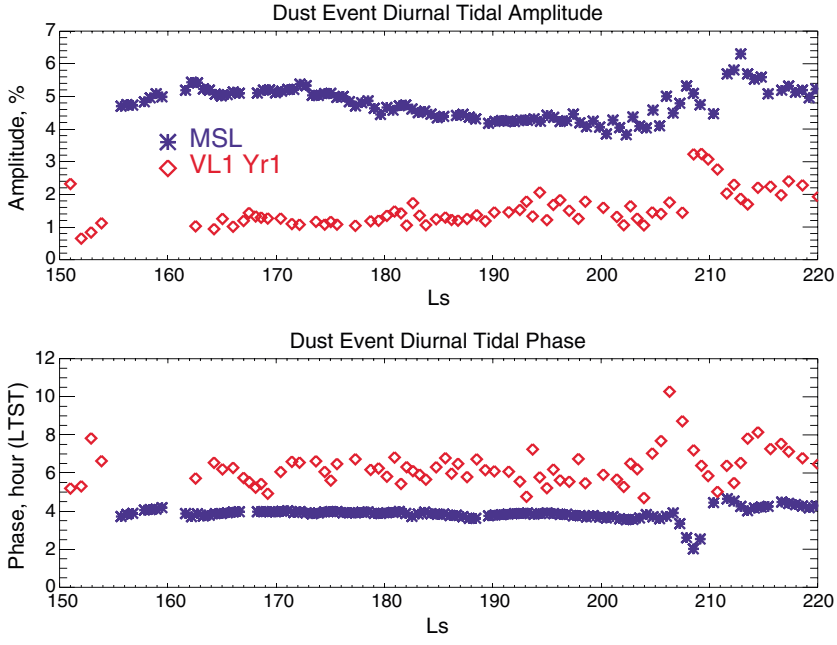

Figure 15. Diurnal amplitude and phase at MSL (blue asterisks) and VL1 Year 1 (red diamonds) for the season corresponding to the first 100 sols of MSL operations.

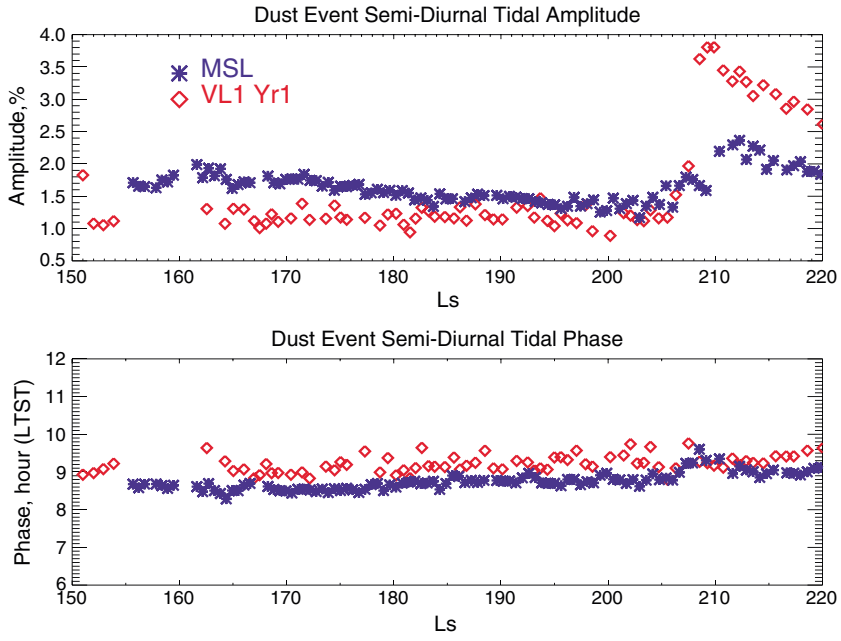

Figure 16. Semidiurnal amplitude and phase at MSL (blue asterisks) and VL1 Year 1 (red diamonds) for the season corresponding to the first 100 sols of MSL operations.

3.7. CO_2 Cycle and Secular Climate Change

The condensation and sublimation of CO_2 in the polar regions during winter and spring causes planetwide fluctuations in the surface pressure, which were first detected by the Viking landers [e.g., *Tillman et al*., 1993]. This CO_2 cycle, which is controlled by the polar heat balance [e.g., *Paige and Ingersoll*, 1985], is best illustrated in the seasonal variation of daily average surface pressure. We show the REMS daily averaged surface pressure during the first 100 sols of the mission in Figure 17. Included for comparison are those measured by the Viking Landers.

As expected REMS arrived at Gale when the daily mean pressures were close to their lowest values of the year. At the arrival season (midsouthern winter) the south polar seasonal cap is at its maximum extent (~40°S), and there is no CO_2 ice cap in the north. As the season progresses, however, the south cap begins to sublime (and retreat) releasing its CO_2 into the atmosphere and increasing global surface pressures. The REMS measurements detected this familiar behavior. Daily mean surface pressure steadily increased during the first 100 sols of the mission, and the rate of increase (~1 Pa/sol) is very similar to that measured by the Viking Landers. The REMS measurements also closely track those at VL-2 because the two landers are at nearly identical elevations (MSL elevation at Bradbury Landing = −4501 m; VL-2 elevation = −4495 m) (Elevation is measured with respect to the topographic datum defined as the mean Martian radius (3382.9 km)). However, upon closer inspection the two data sets diverge near the end of the period with MSL recording lower pressures (Figure 18).

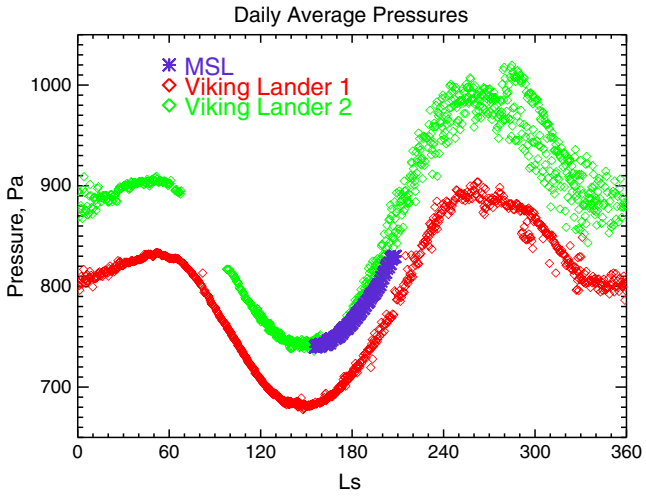

Figure 17. Daily average surface pressures from MSL (blue asterisks), Viking Lander 1 years 1–4 (red diamonds), and Viking Lander 2 years 1–2 (green diamonds).

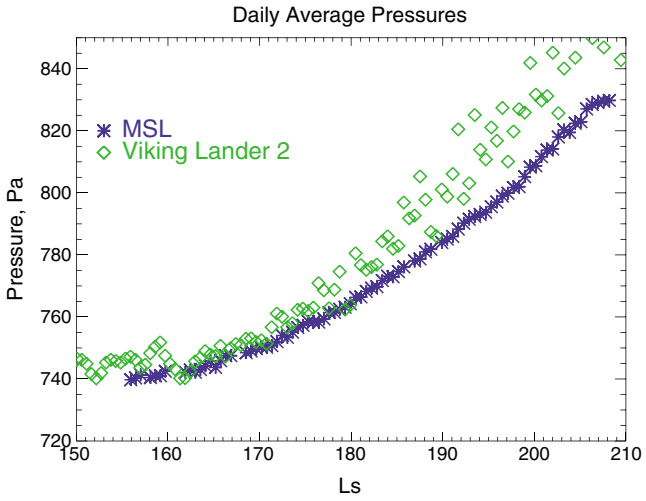

Figure 18. Same as Figure 17 but focused on the first 100 sols of MSL operations and with a comparison only to VL-2.

These lower pressures indicate that factors other than elevation affect the surface pressure. *Hourdin et al.* [1993] were the first to discuss this. They pointed out that pressures are also affected by large-scale topography and atmospheric dynamics. The topographic effect is related to the fact that the northern hemisphere is several kilometers lower on average than the southern hemisphere. Hence, during northern fall and winter when temperatures at northern midlatitudes are much lower (typically near 180 K) than in the southern hemisphere (typically near 230 K), a greater fraction of the atmosphere is trapped in the lower elevations because scale heights are relatively low (~ 9 km for mean temperatures of ~ 180 K). This has the effect of lowering surface pressures in the southern hemisphere and raising them in the northern hemisphere. In effect, denser air is pooling up in the lower elevations of the northern hemisphere at the expense of lower density air at the higher elevations in the southern hemisphere. This topographic effect at least partly explains the higher surface pressures at VL-2 compared to MSL by sol 100 ($Ls \sim 208°$).

However, atmospheric dynamics (i.e., winds) also affects the surface pressure since winds are driven by pressure gradients. During northern fall, temperatures are falling in the northern hemisphere creating an equator-to-pole temperature gradient, which by thermal wind balance requires an increase in westerly winds with height. At this season, the mean meridional circulation extracts angular momentum from the surface in the tropics and transports it to the higher latitudes creating surface westerlies. These low-level westerlies are further reinforced by the developing condensation flow toward the polar cap [e.g., *Leovy and Mintz*, 1969; *Haberle et al.*, 1979, 1993]. Together, these mechanisms create westerlies in northern midlatitudes at all levels, which are supported by lower pressures (on a given equipotential surface) at the poles compared to the equator. Thus, the dynamical effect can partially offset the topographic effect depending on location and season. Based on the observations, the topographic effect appears to be dominant.

This discussion is relevant to the question of secular climate change on Mars, i.e., the possibility that the south polar residual cap (SPRC) is sublimating away with the lost CO_2 going directly into the atmosphere thereby raising global mean surface pressures year after year. *Malin et al.* [2001] first raised this possibility based on Mars Orbiter Camera observations of the changing surface morphology of the SPRC. *Thomas et al.* [2009] conducted more detailed studies in later observations, and *Haberle and Kahre* [2010] searched for and found a possible signal in the Phoenix pressure data. By comparing Phoenix surface pressures with those from Viking, which were acquired about 17 Mars years earlier, and correcting for elevation differences and dynamics (using a model), they found the Phoenix surface pressures to be ~ 10 Pa higher than what would have been expected if there were no systematic increase in atmospheric mass from an eroding SPRC. A similar analysis with REMS data is shown in Figure 19.

The basic idea is to estimate what the surface pressure should have been at Curiosity's location during the Viking mission and then compare that with what we observe today. We estimate surface pressures at Curiosity during the Viking mission by adding to the VL-2 data the altitude-corrected pressure difference between the two sites as determined by the Ames GCM. If today's pressures are different from those estimated during the Viking epoch, then secular climate change is indicated. Based on estimates of the SPRC sublimation rates, pressures should have increased between ~1 and 20 Pa since Viking (VL-2 began measuring surface pressures at $L_s = 150°$ 19 Mars years before MSL landed. *Malin et al.* [2001] estimate erosion rates (likely caused by sublimation) of the SPRC between 0.5 Pa per Mars decade (MD) and 5 Pa/MD. *Blackburn et al.* [2010] find even higher erosion rates (13 Pa/MD). Assuming 80% of the loss goes into the atmosphere (see *Haberle and Kahre* [2010] for details), the estimated pressure change since Viking is $0.05 \times 0.8 \times 19 = 0.76$ Pa for the Malin et al.

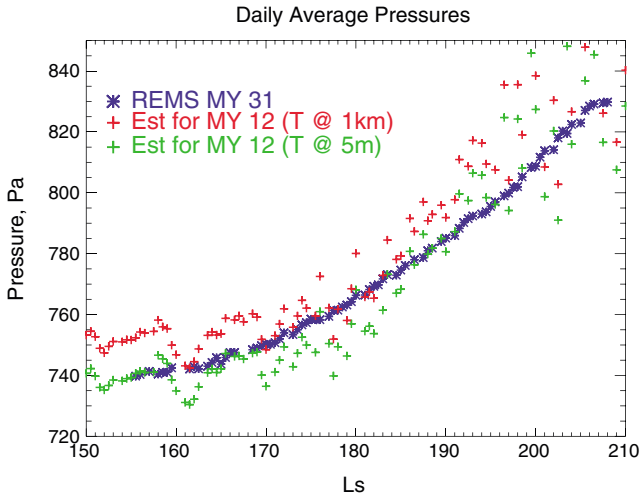

Figure 19. Daily average PS1 pressures (blue asterisks) as measured by REMS during MY 31 and estimates of the daily average pressures at the same location 19 Mars years earlier (MY 12). See text for details. The estimates are based on scale heights calculated with temperatures at 1 km above the surface (red plus symbols) and 5 m above the surface (green plus symbols).

minimum, 7.6 Pa for their maximum, and 19.76 Pa for the *Blackburn et al.* [2010] erosion rate). From Figure 18, however, it appears that mean pressures have changed little since Viking. For the interval from $L_s = 155°$ to $L_s = 208°$ REMS pressures are on average almost identical to those estimated from VL-2 data using the 5 m air temperature interpolation scheme and somewhat lower (~10 Pa) with the 1 km air temperature interpolation scheme. Taken at face value, this suggests there has been very little net erosion of the SPRC since Viking.

However, there are many caveats to this analysis. The main one is our hydrostatic adjustment of simulated surface pressures at the grid point closest to Gale, to the actual landing elevation. The altitude differential is ~ 3.4 km, and as indicated in Figure 18, the adjustment is very sensitive to the assumed temperature profile. This was less of an issue in *Haberle and Kahre* [2010], who were comparing VL-2 with Phoenix, which are in the same hemisphere, nearly the same thermal environment, do not require large hydrostatic adjustments from grid point elevation to actual lander elevation, and neither of which are in a crater. A better approach would be to use pressures from simulations running with high enough spatial resolution to minimize the altitude differential and resolve the crater circulation. Such an effort is underway, and we will report the results in a future paper. It would also be better to wait for a full Mars year of REMS data to compare annual averaged pressures at the two sites. This will minimize the difficulty of removing the topographic effect, which is evident in the data thus far (i.e., REMS daily averaged surface pressures are declining with respect to VL-2 at the end of this period; see Figure 18).

4. Conclusions

The REMS pressure sensor is performing well and revealing information on a variety of meteorological and climatological phenomena. Some of this information is new including an evening oscillation that may be the result of gravity waves, convective vortices that do not lift much dust, and diurnal pressure variations that are much larger than those measured from previous landers. Our preliminary interpretation is that each of these new findings is related to the fact that Curiosity landed at the bottom of a large crater that generates a regional circulation with a noticeable influence on the daily pressure cycle. Nighttime downslope flows along the walls of the crater rim and flanks of Mount Sharp generate gravity waves that induce evening oscillations. During the day the flow reverses generating sinking motion over the crater floor that suppresses the depth of the boundary layer and limits the peak intensity of the convective vortices. Combined, these upslope/downslope flows export/import air from the crater and amplify the already large diurnal variation in pressure expected from the global thermal tides at Curiosity's location.

More familiar findings from the REMS pressure data include the sensitivity of the tides to dust loading and the expected progression of the seasonal CO_2 cycle. The ramping up of the diurnal and semidiurnal amplitudes around $L_s = 200°$ follows the pattern seen by the Viking Landers in 1977 and is attributable to the development of a regional dust storm in the southern hemisphere not far from Gale Crater. However, this storm remained regional and did not become planet-encircling as did the first one in 1977. Consequently, REMS tidal amplitudes peaked at smaller values than Viking. Also, prior to the storm REMS tidal amplitudes were in decline, which was different from the Viking observations and is interpreted to be the result of the declining influence of the Kelvin wave at this season since observed dust loadings were relatively steady during this period.

The increase in daily average surface pressures seen by REMS during this season is due to the retreat of the south polar cap. The rate of change in daily average surface pressure closely follows that of previous landers suggesting a very repeatable seasonal CO_2 cycle. And the fact that Curiosity and VL-2 are at nearly identical elevations should help with assessing the potential for secular climate change. Based on the first 100 sols of REMS data, however, there is no evidence for an increase in mean pressures since Viking. However, because the two landers are in very different thermal and geographical environments, their seasonal cycles will not be identical. For this reason, it is best to wait for higher-resolution GCM simulations and a full Mars year of REMS data before drawing any definitive conclusion about secular climate change.

Acknowledgments

NASA's Mars Exploration Program and Planetary Science Division supported this work. J. G.-E., J. M.-T., J. A. R.-M., and M.-P. Z. are supported by Economy and Competitivity Ministry (AYA2011-25720). The reviews of A. Spiga and R. J. Wilson greatly improved the manuscript. R. M. H. acknowledges Dan Tyler and Jeff Barnes for their stimulating discussions about crater circulations.

References

Blackburn, D. G., K. L. Bryson, V. F. Chevrier, L. A. Roe, and K. G. White (2010), Sublimation kinetics of CO_2 ice on Mars, *Planet. Space Sci.*, *58*, 780–791, doi:10.1016/j.pss.2009.12.004.

Ellehøj, M. D., et al. (2010), Convective vortices and dust devils at the Phoenix Mars mission landing site, *J. Geophys. Res.*, *115*,E00E16, doi:10.1029/2009JE003413.

Golombek, M., et al. (2012), Selection of the Mars Science Laboratory landing site, *Space Sci. Rev.*, *170*, 641–637, doi:10.1007/s11214-012-9916-y.

Gómez-Elvira, J., et al. (2012), REMS: The environmental sensor suite for the Mars Science Laboratory rover, *Space Sci. Rev.*, *170*, 583–640, doi:10.1007/s11214-012-9921-1.

Grotzinger, J. P., et al. (2012), Mars Science Laboratory mission and science investigation, *Space Sci. Rev.*, *170*, 5–56, doi:10.1007/s11214-012-9892-2.

Haberle, R. M., and M. A. Kahre (2010), Detecting secular climate change on Mars, *Mars*, *5*, 68–75, doi:10.1555/mars.2010.0003.

Haberle, R. M., C. B. Leovy, and J. B. Pollack (1979), A numerical model of the Martian polar cap winds, *Icarus*, *39*, 151–183.

Haberle, R. M., J. B. Pollack, J. R. Barnes, R. W. Zurek, C. B. Leovy, J. R. Murphy, and J. Schaeffer (1993), Mars atmospheric dynamics as simulated by the NASA Ames General Circulation Model, I—The zonal-mean circulation, *J. Geophys. Res.*, *98*, 3093–3123.

Haberle, R. M., et al. (2013), Meteorological predictions for the first 100 sols of the REMS experiment on MSL, *Mars*, in press.

Harri, A.-M., et al. (2014), Pressure observations by the Curiosity rover: Initial results, *J. Geophys. Res. Planets*, *119*, doi:10.1002/2013JE004423.

Holton, J. R. (2004), *An Introduction to Dynamic Meteorology*, 4th ed., Elsevier Academic Press, Burlington, MA.

Hourdin, F., P. L. Van, F. Forget, and O. Talagrand (1993), Meteorological variability and the annual surface pressure cycle on Mars, *J. Atmos. Sci.*, *50*, 3625–3640.

Kahanpää, H., et al. (2013), Convective vortices in Gale Crater, *44th Lunar and Planet. Sci. Conf.*, paper No. 3095.

Leovy, C. B., and Y. A. Mintz (1969), Numerical simulation of the atmospheric circulation and climate of Mars, *J. Atmos. Sci.*, *26*, 1167–1190.

Leovy, C. B., and R. W. Zurek (1979), Thermal tides and Martian dust storms: Direct evidence for coupling, *J. Geophys. Res.*, *84*, 2956–2968.

Madeleine, J.-B., F. Forget, E. Millour, T. Navarro, and A. Spiga (2012), The influence of radiatively active water ice clouds on the Martian climate, *Geophys. Res. Lett.*, *39*, L23202, doi:10.1029/2012GL053564.

Malin, M. C., M. A. Caplinger, and S. D. Davis (2001), Observational evidence for an active surface reservoir of solid carbon dioxide on Mars, *Science*, *294*, 2146–2148.

Michaels, T. I., and S. C. R. Rafkin (2004), Large-Eddy simulation of atmospheric convection on Mars, *Q. J. R. Meteorol. Soc.*, *130*, 1251–1274.

Moores, J. E., et al. (2013), Constraints on atmospheric water vapor and circulation at gale Crater from the MSL atmospheric monitoring campaign, *44th Lunar and Planet. Sci. Conf.*, Paper No. 1548.

Paige, D. A., and A. P. Ingersoll (1985), Annual heat balance of the Martian polar caps: Viking observations, *Science*, *228*, 1160–1168, doi:10.1126/science.228.4704.1160.

Rennó, N. O., M. L. Burkett, and M. P. Larkin (1998), A simple theory for dust devils, *J. Atmos. Sci.*, *55*, 3244–3252.

Rennó, N. O., A. A. Nash, J. Luninne, and J. Murphy (2000), Martian and terrestrial dust devils: Test of a scaling theory using Pathfinder data, *J. Geophys. Res.*, *105*, 1859–1866, doi:10.1029/19999JE001037.

Schofield, J. T., J. R. Barnes, D. Crisp, R. M. Haberle, S. Larsen, J. A. Magalhães, J. R. Murphy, A. Seiff, and G. Wilson (1997), The Mars Pathfinder atmospheric structure Investigation/Meteorology (ASI/MET) Experiment, *Science*, *278*, 1752, doi:10.1126/science.278.5344.1752.

Spiga, A., and F. Forget (2009), A new model to simulate the Martian mesoscale and microscale atmospheric circulation: Validation and first results, *J. Geophys. Res.*, *114*, E02009, doi:10.1029/2008JE003242.

Spiga, A., F. Forget, B. Dolla, S. Vinatier, R. Melchiorri, P. Drossart, A. Gendrin, J.-P. Bibring, Y. Langevin, and B. Gondet (2007), Remote sensing of surface pressure on Mars with the Mars Express/OMEGA spectrometer: 2. Meteorological maps, *J. Geophys. Res.*, *113*, E08S16, doi:10.1029/2006/JE002870.

Thomas, P. C., P. B. James, W. M. Calvin, R. Haberle, and M. C. Malin (2009), Residual south polar cap of Mars: Stratigraphy, history, and implications of recent changes, *Icarus*, *203*, 352–375, doi:10.1016/j.icarus.2009.05.014.

Tillman, J. E., N. C. Johnson, P. Guttorp, and D. B. Percival (1993), The Martian annual atmospheric pressure cycle: Years without great dust storms, *J. Geophys. Res.*, *84*, 10,963–10,971.

Toigo, A. D., M. I. Richardson, S. P. Ewald, and P. J. Gierasch (2003), Numerical simulation of Martian dust devils, *J. Geophys. Res.*, *108*(E6), 5047, doi: 10.1029/2002JE002002.

Tyler, D., Jr., and J. R. Barnes (2013), Mesoscale modeling of the circulation in the Gale Crater region: An investigation into the complex forcing of convective boundary layer depths, *Mars*, *8*, 58–77, doi:10.1555/mars.2013.0003.

Vasavada, A. R., et al. (2012), Assessment of environments for Mars Science Laboratory entry, descent, and surface operations, *Space Sci. Rev.*, *170*, 793–835, doi:10.1007/s11214-012-9911-3.

Wilson, R. J., and K. Hamilton (1996), Comprehensive model simulation of thermal tides in the Martian atmosphere, *J. Atmos. Sci.*, *53*, 1290–1326.

Wilson, R. J., S. R. Lewis, L. Montabone, and M. D. Smith (2008), Influence of water ice clouds on Martian tropical atmospheric temperatures, *Geophys. Res. Lett.*, *35*, L07202, doi:10.1029/2007GL032405.

Zurek, R. W. (1976), Diurnal tide in the Martian atmosphere, *J. Atmos. Sci.*, *33*, 321–337.

Zurek, R. W. (1981), Influence of dust opacities for the 1977 Martian great dust storms from Viking Lander pressure data, *Icarus*, *45*, 202–215.